

Synthesis, x-ray structure and spectroscopic and electronic properties of two new synthesized flavones

Nicole Cotelle,^{1*} Laurence Vrielynck,² Guy Nowogrocki,³ Philippe Cotelle⁴ and Hervé Vezin⁴

¹Laboratoire de Chimie Organique et Macromoléculaire, Equipe Polyphénols, UMR CNRS 8009, USTL, 59655 Villeneuve d'Ascq Cedex, France

²Laboratoire de Spectrochimie Infrarouge et Raman, UMR CNRS 8516, USTL, 59655 Villeneuve d'Ascq, Cedex, France

³Laboratoire de Cristallographie et Physicochimie du solide, UMR CNRS 8012, ENSCL, BP108 59652, Villeneuve d'Ascq Cedex, France

⁴Laboratoire de Chimie Organique et Macromoléculaire, Equipe Molécules Pro et Antioxydantes, UMR, CNRS 8009, USTL, 59655 Villeneuve d'Ascq Cedex, France

Received 9 November 2002; revised 5 September 2003; accepted 3 October 2003

ABSTRACT: Two new flavones (**1** and **2**) in which one or two di-*tert*-butylhydroxyphenyl groups replace the B-ring of flavonoids, respectively, were synthesized according to the Baker–Vankataraman method. Their crystal structures were determined by x-ray diffraction methods and compared with those obtained by theoretical calculations using joint Monte Carlo conformational search analysis and geometry optimization *ab initio* formalism. NMR NOE data, ESR spectra and electronic properties were obtained in order to understand their implication in the enhancement of low-density lipoprotein (LDL) resistance to oxidation. The oxidative modification of LDL has been alleged to play an important role in the development of human atherosclerosis and neurodegenerative diseases. Copyright © 2004 John Wiley & Sons, Ltd.

KEYWORDS: flavones; crystal structure; electronic properties; low-density lipoprotein

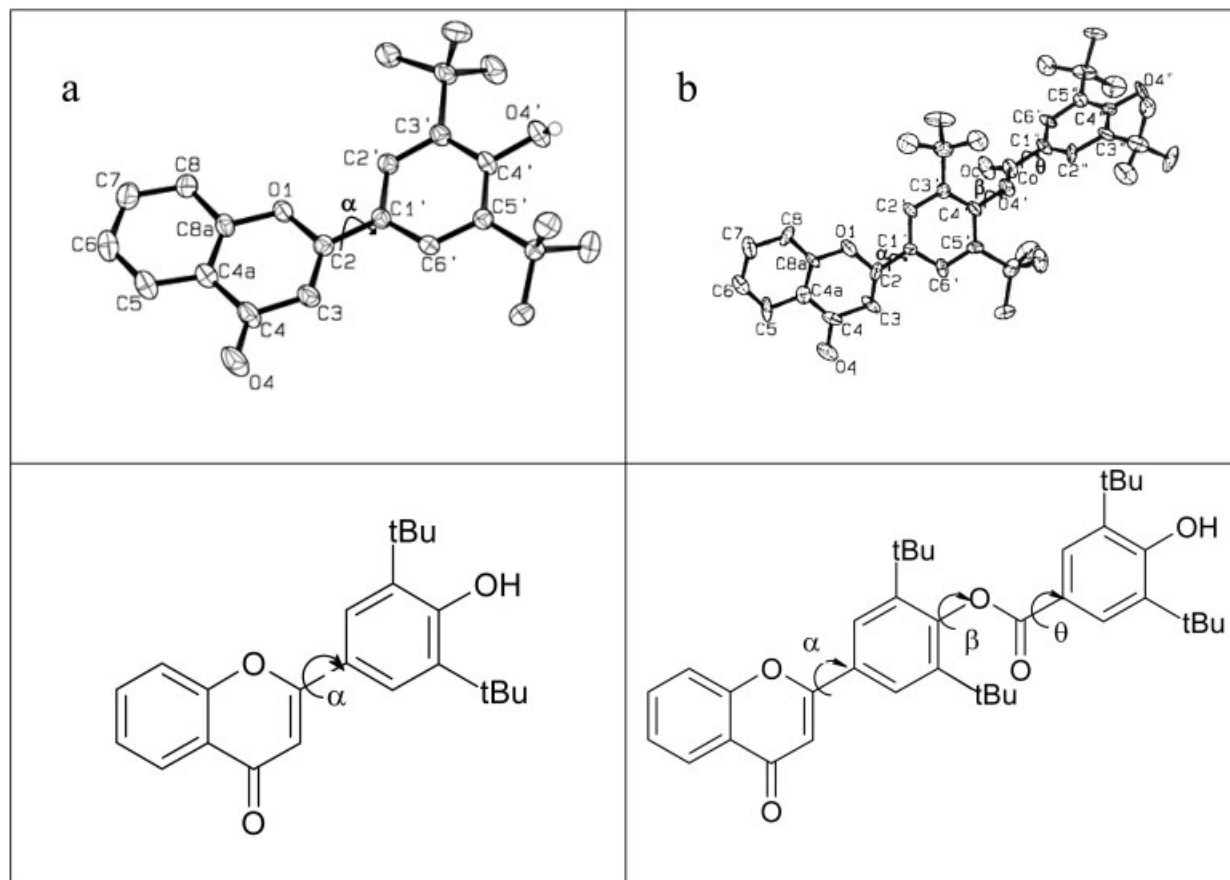
INTRODUCTION

Flavonoids are a group of low molecular weight natural molecules widely distributed in the plant kingdom, and represent a significant part of the average Western daily diet. Flavonoids are benzo- γ -pyrone derivatives and consist of a benzene ring (commonly named A ring) attached to a six-membered heterocycle (named C-ring), which carries at C-2 a phenyl group (named B ring) as a substituent. The most commonly occurring flavones and flavonols are those hydroxylated at positions 5 and 7 (A-ring) and 3' and 4' (B-ring). Among this family of polyphenols, the flavones exhibit a wide variety of biological properties. Indeed, most of them have been found to possess anti-ischemic,¹ antiplatelet,² anti-inflammatory^{3,4} or antilipoperoxidant⁵ activities. Flavones are also well known to inhibit a wide range of enzymes involved in oxidation systems.^{6–9} These polyphenolic compounds can exert their antioxidant activity by various mechanisms, e.g. by scavenging radicals, by binding metal ions, but also by inhibiting enzymatic systems responsible for free radical generation. In contrast to the beneficial effects, some flavones with catechol or pyrogallol moieties have also been reported to be mutagenic.^{10,11} In order to prevent these problems, we

have synthesized two new flavones in which the di-*tert*-butylhydroxyphenyl group replaces the catechol moiety. This motif is present in butylated hydroxytoluene (BHT), which is well known for its antioxidant properties and widely used in the USA as a food additive. Nevertheless, the presence of one or several di-*tert*-butylhydroxyphenyl groups may cause drastic constraints in the molecular structure and consequently could affect the binding mode to enzymes involved in oxidation systems, e.g. lipoxigenases, cyclooxygenases, monooxidase and xanthine oxidase.

In this work, we first performed a structural analysis by x-ray diffraction of the two new synthesized flavones (**1** and **2**) exhibiting two *tert*-butyl-substituted groups on the B ring in the 3' and 5' positions. The structures of both molecules are shown in Scheme 1(a) and (b), respectively, and **2** differs from **1** by the presence of the D ring which bears two *m-tert*-butyl groups and is linked to the B ring through an ester function. The results of a quantum chemical conformational analysis, performed at the isolated molecule level with the *ab initio* 3–21G* formalism, are reported and compared with the crystallographic data. Subsequently, we focused on many specific spectroscopic properties of **1** and **2**, especially the electronic properties, which may be helpful in understanding the structure–activity relationship for these kinds of compounds. ESR spectroscopic experiments on radical formation analysis were performed in order to understand the mechanism of radical scavenging. We performed

*Correspondence to: N. Cotelle, Laboratoire de Chimie Organique et Macromoléculaire, Equipe Polyphénols, UMR CNRS 8009, USTL, 59655 Villeneuve d'Ascq Cedex, France.
E-mail: nicole.cotelle@univ-lille1.fr



Scheme 1. Structures of (a) **1** and (b) **2** with atom numbering

molecular modeling in order to understand the structural differences induced by the addition of one or two BHT templates, respectively, at the 2'-position on the C ring of the flavone molecule.

Finally, the antioxidant biological properties of **1** and **2**, i.e. protection of low-density lipoprotein (LDL) from oxidation, were compared with theoretical calculations particularly with the HOMO energy and its distribution on the molecule.

RESULTS AND DISCUSSION

Chemistry

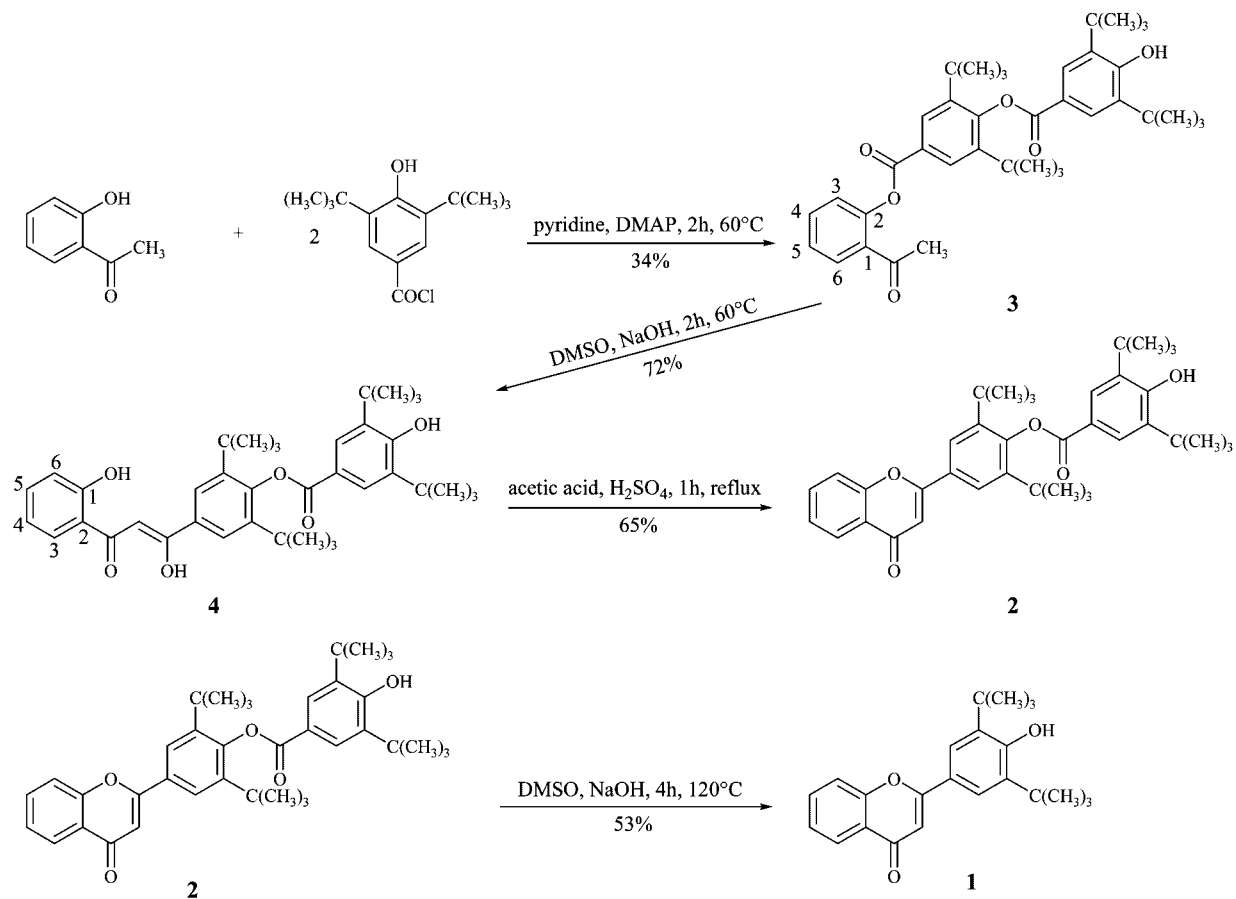
Compounds **1** and **2** were prepared as previously described according to the Baker–Vankataraman procedure^{12,13} (Scheme 2). The 2-hydroxyacetophenone was condensed with 3,5-di-*tert*-butyl-4-hydroxybenzoyl chloride in the presence of dimethylaminopyridine in dry pyridine at 60°C for 2 h to give the diester **3** in 34% yield. This result was not surprising since 3,5-di-*tert*-butyl-4-hydroxybenzoyl chloride reacted in dry pyridine at 60°C to give 4-(3,5-di-*tert*-butyl-4-hydroxybenzoyloxy)-3,5-di-*tert*-butylbenzoic acid in 60% yield. The diester **3** was treated with sodium hydroxide in dry

DMSO to give the diarylpropane-1,3-dione **4** in 72% yield. The cyclization of **4** was carried out under reflux in acetic acid in the presence of sulfuric acid for 1 h, leading to **2** in 65% yield. Compound **2** was saponified with sodium hydroxide in dry DMSO for 4 h at 120°C to give **1** in 53% yield.

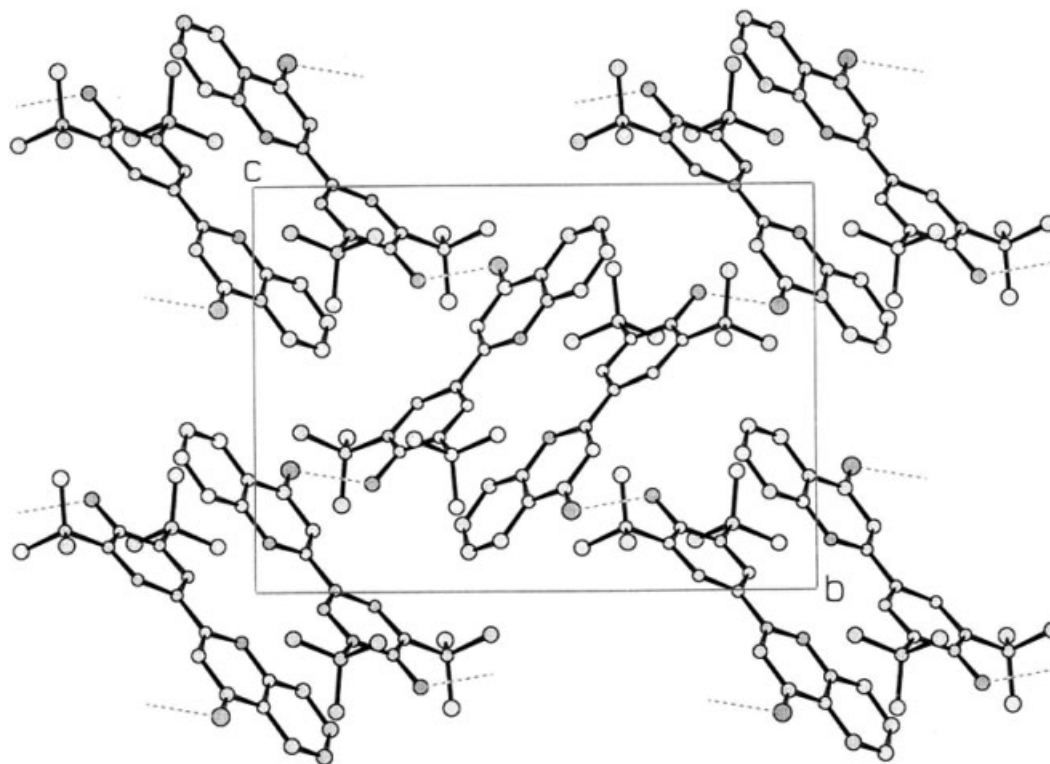
Crystal structures

The molecular packings of **1** and **2** are shown in Figs 1 and 2, respectively. The experimental crystallographic parameters of both molecules are summarized in Table 1. Selected bond lengths and angles are listed in Table 2.

In **1**, which crystallizes in the $P2_1/n$ space group, a medium–strong intermolecular hydrogen bonding interaction was found between the O4 carbonyl oxygen atom of a molecule and the hydrogen atom of the hydroxyl group of a neighboring molecule, which are both related by a glide plane. The intermolecular distances $O4 \cdots O4'$ and $O4 \cdots H(O4')$ are 2.658(4) and 1.89(4) Å, respectively, and the angle $O4 \cdots H(O4')$ is reported to be 153°. These intermolecular hydrogen links entail the formation of infinite chains roughly parallel to the $[1 -1 0]$ direction. All other intermolecular distances are >3.3 Å. The presence of a symmetry center creates pairs of



Scheme 2. Synthetic pathway

Figure 1. Projection on the (*b*,*c*) plane of the **1** structure

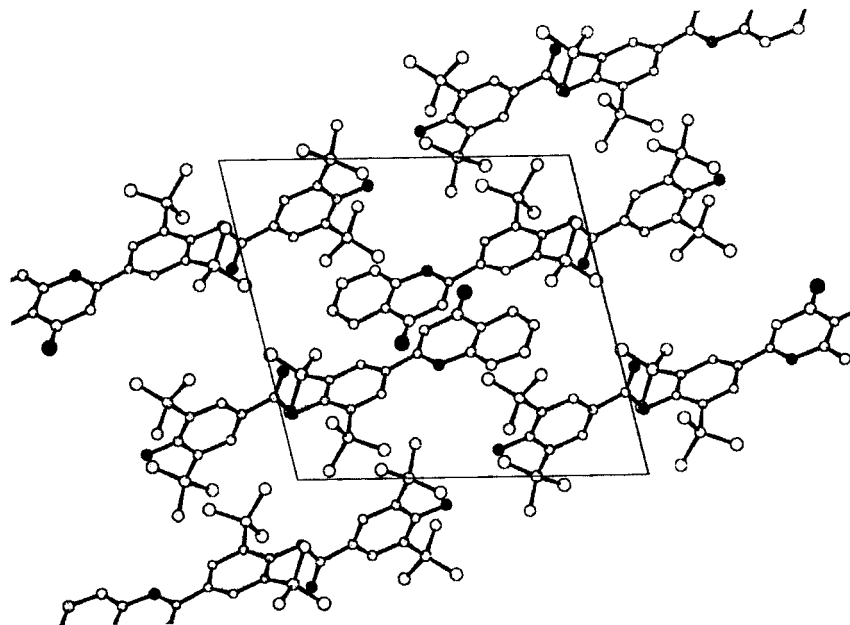


Figure 2. Projection on the (a,b) plane of the **2** structure

quasi-parallel molecules which are about 3.5 Å apart and for which the carbon skeletons undergo severe geometric distortions as the result of the bulky *tert*-butyl groups on the phenyl B ring [Fig. 3(a)]. Eventually, the intermolecular hydrogen bridges essentially stabilize the three-dimensional network.

In **2**, which crystallizes in the $P-1$ space group, the shortest intermolecular distance occurs between the $O4''$

carbonyl oxygen atoms of two molecules which are related by a symmetry center at 3.11 Å, suggesting a very weak hydrogen bonding interaction. The next shortest distance (3.46 Å) occurs between parallel aromatic rings where some strong π - π interactions are involved [Fig. 3(b)], thus allowing stabilization of the crystal lattice.

The structures of **1** and **2** are essentially controlled by the value of specific dihedral angles such as α ($C3-C2-C1'-C6'$) for **1** and **2** and β ($C5'-C4'-O4'-Cc$) and θ ($Oc-Cc-C1''-C2''$) for **2**, which describe the principal degrees of freedom in these two molecules.

The small α torsion angle value in **1**, measured as 1.7°, appears to favor the π system delocalization between the B ring and the γ -pyrone part, although in **2** the conjugation is strongly restricted owing to an angle value of almost 6°. In **2**, the reported bond lengths for $C2-C1'$ (1.474 Å) and $C3-C4$ (1.444 Å) show that these bonds exhibit single-bond character, even though the $C2-C3$ bond, which is very short (1.333 Å), presents an obvious double bond order. The non-coplanarity of the phenyl ring and the benzopyrone moiety supports a decrease in the conjugation between the $C2-C1'$ bond and the π electrons of the γ -pyrone ring. In **2**, the value of the dihedral angle $C5'-C4'-O4'-Cc$ that is reported to be close to 100° and can be explained by the strong steric hindrance of the *tert*-butyl motifs on the B ring. The carbonyl bond $Cc-Oc$ is short (1.200 Å) and does not appear to be conjugated with this phenyl D ring as suggested by the single-bond character of the $Cc-C1''$ bond (1.472 Å). The low conjugation of the carbonyl group is also confirmed by a dihedral angle θ value of -168.3° measured from x-ray data indicating the out-of-plane position of the CO group. Moreover, *ab initio* calculations also show that for all the theoretical

Table 1. Crystal data and details of data collections

Compound	1	2
Formula	$C_{23}H_{26}O_3$	$C_{38}H_{46}O_5$
Formula weight ($g\ mol^{-1}$)	350.44	582.75
Space group	$P2_1/n$	$P-1$
Crystal size (mm^3)	$0.35 \times 0.30 \times 0.25$	$0.30 \times 0.15 \times 0.10$
a (Å)	10.164 (4)	14.317 (3)
b (Å)	16.135 (7)	13.338 (3)
c (Å)	12.090 (5)	9.434 (2)
α (°)	90.0	104.22 (3)
β (°)	99.909 (9)	97.86 (3)
γ (°)	90.0	100.86 (3)
V (Å ³)	1953 (1)	1683.2 (6)
Z	4	2
Linear absorption coefficient ($\mu\ mm^{-1}$)	0.077	0.075
D_c ($g\ cm^{-3}$)	1.192	1.150
θ limits	2–31	3.2–25.0
hkl limits	-14, 14; -23, 23; -17, 16	-17, 17; -15, 15; -11; 11
No. of data collected	16505	11719
No. of intensities	5281	5847
No. of intensities $I > 2\sigma(I)$	2537	2578
R	0.0439	0.0514
R_w	0.1055	0.1098
Goodness of fit	0.851	1.049
No. of variables	313	527

Table 2. Bond length and angles from x-rays diffraction and 3-21G* *ab initio* data^a

	Bond length (Å)				Bond angle (°)				Dihedral angles (°)					
	1		2		1		2		1		2			
	3-21G	X-ray	3-21G	X-ray	3-21G	X-ray	3-21G	X-ray	3-21G	X-ray	3-21G	X-ray		
O1—C8a	1.375	1.380	1.375	1.377	O1—C8a—C8	117.0	116.1	118.0	116.1	O1—C2—C3—C4	0.4	-3.2	-0.2	2.4
O1—C2	1.373	1.356	1.371	1.353	C8a—C8—C7	118.9	118.9	118.8	118.9	C2—C3—C4—O4	179.2	-178.9	-179.0	179.6
C2—C3	1.333	1.349	1.331	1.333	C8—C7—C6	120.7	120.5	120.7	120.6	C2—C3—C4—C4a	-0.8	-1.4	0.2	-2.2
C3—C4	1.456	1.436	1.458	1.444	C7—C6—C5	119.9	120.2	120.7	119.8	C3—C4—C4a—C8a	-0.1	3.5	-0.7	0.4
C4—C4a	1.475	1.453	1.474	1.456	C6—C5—C4a	120.4	120.8	120.3	121.4	C4—C4a—C5—C6	-179.9	178.5	-179.7	178.4
C4—O4	1.240	1.246	1.240	1.236	C5—C4a—C4	122.0	123.6	120.5	123.6	C4a—C5—C6—C7	0.0	0.1	-0.1	1.7
C8a—C4a	1.377	1.383	1.377	1.37	O1—C2—C3	120.7	120.9	121.0	120.7	C5—C6—C7—C8	0.0	0.1	0.0	-0.02
C8a—C8	1.385	1.384	1.384	1.38	C2—C3—C4	122.5	122.3	122.3	122.9	C6—C7—C8—C8a	0.0	-0.9	0.1	-0.06
C8—C7	1.376	1.369	1.376	1.371	C3—C4—C4a	114.3	115.7	114.3	114.9	O1—C2—C1'—C2'	3.93	1.3	15.93	-4.6
C7—C6	1.394	1.388	1.394	1.376	C3—C4—O4	123.0	123.4	123.0	122.8	C2—C1'—C2'—C3'	179.0	174.3	-173.2	-177.2
C6—C5	1.374	1.362	1.374	1.351	C3—C2—C1'	127.2	127.7	127.0	127.8	C1'—C2'—C3'—C4'	0.1	0.8	3.2	3.6
C5—C4a	1.389	1.407	1.390	1.404	C2—C1'—C2'	119.5	120.1	119.3	119.5	C2'—C3'—C4'—C5'	0.2	2.8	-5.9	-9.0
C2—C1'	1.470	1.476	1.475	1.474	C1'—C2'—C3'	121.5	122.4	122.0	122.4	C3'—C4'—C5'—C6'	-0.2	-4.1	4.6	7.5
C1'—C2'	1.381	1.387	1.385	1.389	C2'—C3'—C4'	117.7	117.3	116.6	115.5	C4'—C5'—C6'—C1'	0.0	1.9	-0.3	-0.5
C2'—C3'	1.382	1.388	1.391	1.388	C3'—C4'—C5'	122.1	122.5	123.0	124.5	C1'—C2'—C3'—C(CH ₃)	180.0	-176.7	-177.0	-174.0
C3'—C4'	1.397	1.406	1.391	1.395	C4'—C5'—C6'	117.5	116.6	117.3	115.5	C1'—C6'—C5'—C(CH ₃)	-179.9	-180	176.9	177.4
C4'—O4'	1.376	1.376	1.407	1.417	C5'—C6'—C1'	122.0	122.6	121.4	122.5	C6'—C5'—C4'—O4'	180.0	179.7	-176.1	-177.0
C4'—C5'	1.402	1.411	1.403	1.404	C5'—C4'—O4'	115.8	120.7	116.9	117.2	C5'—C4'—O4'—H	-178.6	-61.7		
C5'—C6'	1.379	1.393	1.381	1.387	C2'—C3'—C(CH ₃)	120.4	120.5	117.0	119.1	C4'—O4'—O4'—Cc			101.5	99.7
C6'—C1'	1.389	1.391	1.396	1.377	C6'—C5'—C(CH ₃)	121.0	120.3	120.1	120.8	C4'—O4'—Cc—Oc			0.7	-0.3
C3'—C(CH ₃)	1.544	1.546	1.550	1.546	C4'O4'H	114.6	113.4			O4'—Cc—C1'—C2''			-2.4	12.5
C5'—C(CH ₃)	1.510	1.544	1.550	1.542	C4'—O4'—Cc			120.0	117.1	Oc—Cc—C1'—C2''			177.5	-168.3
C—CH ₃	1.541	1.53	1.550	1.53	O4'—Cc—Oc			125.7	122.7	Cc—C1'—C2''—C3''			179.0	175.3
O4'—H	0.957	0.8350			Cc—C1'—C2''			122.8	123.0	C1''—C2''—C3''—C4''			0.0	1.8
O4'—Cc			1.375	1.373	Oc—Cc—C1'			128.0	125.7	C2''—C3''—C4''—C5''			0.0	0.9
Cc—Oc			1.204	1.200	C1''—C2''—C3''			121.2	122.0	C3''—C4''—C5''—C6''			0.3	-3.1
Cc—C1''			1.468	1.472	C2''—C3''—C4''			117.5	116.5	C6''—C5''—C4''—O4''			-179.0	177.4
C1''—C2''			1.388	1.388	C3''—C4''—C5''			122.5	123.8	C1''—C6''—C5''—C(CH ₃)			179.5	-179.7
C2''—C3''			1.401	1.376	C4''—C5''—C6''			117.4	116.6	C1''—C2''—C3''—C(CH ₃)			-179.8	-177.5
C3''—C4''			1.418	1.403	C5''—C4''—O4''			121.7	117.2					
C4''—C5''			1.402	1.405	C2''—C3''—C(CH ₃)			120.0	120.8					
C5''—C6''			1.402	1.388	C6''—C5''—C(CH ₃)			120.7	120.1					
C6''—C1''			1.390	1.389	C3''—C—CH ₃			110.0	111.2					
C4''—O4''			1.371	1.374	C5''—C—CH ₃			110.0	110.8					
C3''—C(CH ₃)			1.543	1.532										
C5''—C(CH ₃)			1.542	1.542										
C—CH ₃			1.550	1.53										

^a Standard deviations are about 0.002 Å and 0.2° for **1** and 0.004 Å and 0.2° for **2**. Intermolecular parameters: **1**, O4'...O4 = 2.658 Å, H...O4 = 1.89 Å and O4'H...O4 = 152.7°; **2**, O4''...O4'' = 3.11 Å, Oc...C6 = 3.22 Å.

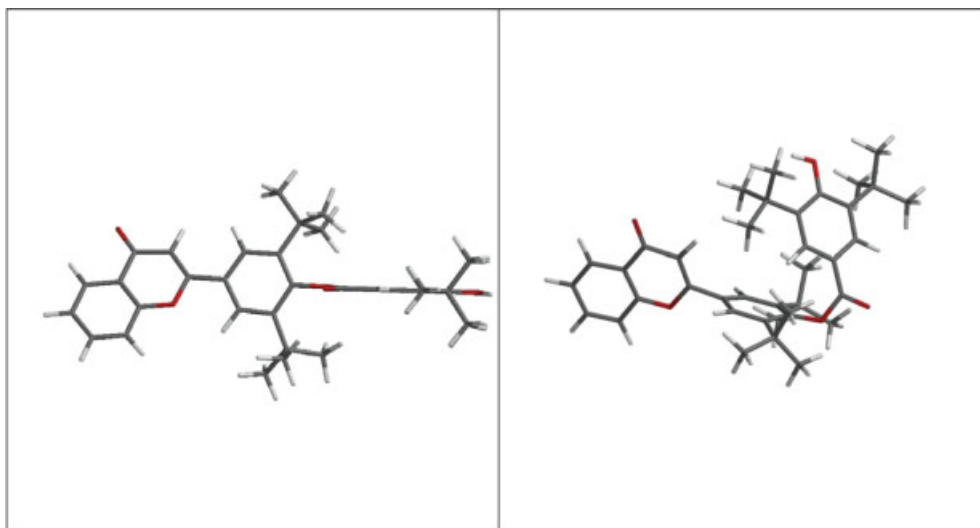


Plate 1. Structures of the most stable conformers of **2**: **2₁** (left) corresponding to the x-ray structure and **2₂** (right) to the folded structure. Structures were obtained by Monte Carlo analysis and then fully optimized at the Hartree–Fock level with the 3–21G* basis set

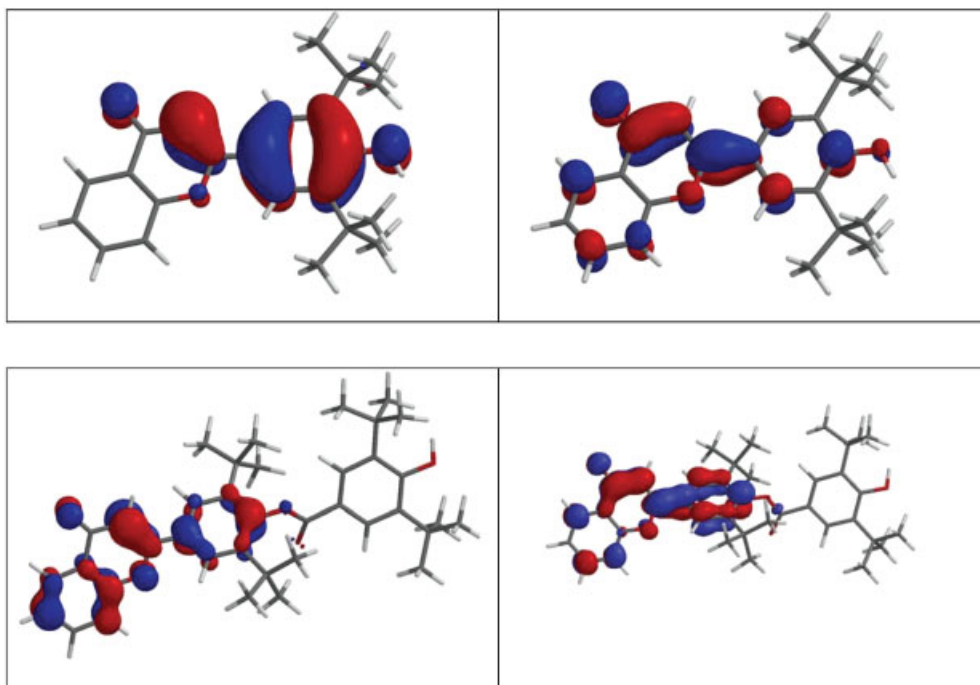


Plate 2. Three-dimensional contour plot for the molecular orbital HOMO (left) and LUMO (right) for **1** (top) and **2₁** conformer molecule (bottom)

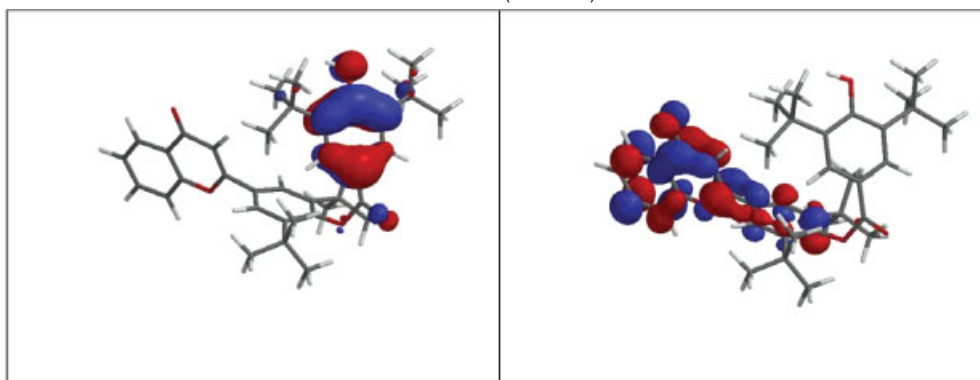


Plate 3. Three-dimensional contour plot for the molecular orbital HOMO (left) and LUMO (right) for the **2₂** conformer

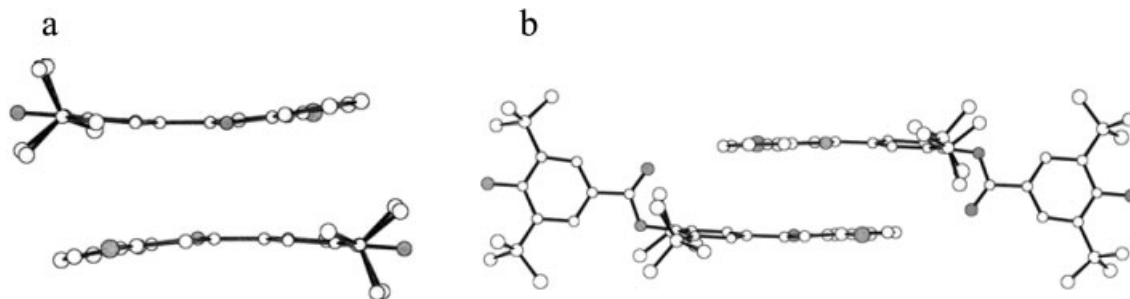


Figure 3. Stacking of molecules to show the quasi-parallelism of benzopyran groups for (a) **1** and (b) **2**

conformers these values are far from that for the planar structure of this CO bond (Table 3).

Computational chemistry

The Monte Carlo conformational analysis of **2** revealed nine series of stable conformers resulting from the energy global minimum search, which are all characterized by different values of θ , α and β angles. Each conformer was then fully optimized at the Hartree–Fock level using a 3–21G* basis set. Two groups of structures with a heat of formation of $-162.36 \text{ kcal mol}^{-1}$ (1 kcal = 4.184 kJ) (two structures) and $-164.0 \text{ kcal mol}^{-1}$ (two structures) respectively for **2** (Plate 1) were obtained from these calculations. Only one structure with a heat of formation of $-84.33 \text{ kcal mol}^{-1}$ was found for **1**. The first **2** conformer of $-162.36 \text{ kcal mol}^{-1}$ corresponds to the crystallographic structure whereas that of $-164.0 \text{ kcal mol}^{-1}$ is related to a folded structure, folding between the D and B rings. The main differences found in this spatial structure arise from drastic changes in the θ , α and β angle values and are displayed in Table 3. At this stage we hypothesized that this folded structure may reflect the possible conformation in solution where the π – π interaction found in the crystal structure is vanishes. NMR steady-state NOE experiments tend to confirm the reality of these structures. Irradiation of the signal of hydrogen H3 of **2** produced a strong NOE (27%) of the signal of hydrogens H2' and H6'. Conversely, a strong NOE of approximately same value (34%) was observed for the signal of hydrogen H3 when H2'/H6' were irradiated. However, in

solution, the NMR results show the equivalence of hydrogens (and carbons) on symmetry-related sites of the phenyl B and D rings and also for those of the 3', 5'- and 3'', 5''-*t*-Bu groups. Thus rapid exchange occurs on the NMR time-scale between all these pairs of sites through rotation around the single bonds C2–C1', C4'–O4', Cc–C1''. The mean distances between H2', H6' and H3 do not differ significantly in the two conformers envisaged, **2**₁ and **2**₂, hence NOE does not allow are to make a choice between the conformations.

The average of inter-proton distance in conformer **2**₂ is related to a modification of the α dihedral angle value. The main geometric features resulting from the energy global minimum search (for **1** and **2**) are reported in Table 2. The presence of the *tert*-butyl groups in the 3' and 5' positions on the B ring of **1** and **2** leads to a torsion angle ($O_1C_2C_1, C_2$) of the B ring with the rest of the molecule (A and C rings) close to 1 ± 0.3 and $4.1 \pm 0.4^\circ$ (Table 2). This means that **1** and **2** are almost planar. It has been stated in general that the flavone B ring is slightly ($\pm 20^\circ$) twisted relative to the plane of the A and C rings. For example, apigenin (5,7,4'-trihydroxyflavone) presents a torsion angle of 16.48° , unlike flavonols, which are planar, e.g. quercetin (3,5,7,3',4'-pentahydroxyflavone) presents a torsion angle of -0.29° . The cause of the planarity of the flavonols appears to be a hydrogen bond-like interaction between the 3-OH and 2'- or 6'-proton.¹⁴

For conformers **1** and **2**₁, good agreement is observed between the calculated geometric parameters and the crystallographic data, notably for distances and valence angles.

Table 3. Energy formation and dihedral angle values for the two sets of conformer for **2**: **2**₁ related to crystallographic structure and **2**₂ to folded conformation^a

	Heat of formation (kcal mol ⁻¹)	α (°)	β (°)	θ (°)
2 ₁	-162.36	4.1	101.5	177.5
	-162.35	-4.3	-101.6	147.0
2 ₂	-164.09	-105.8	83.5	-130.9
	-163.9	60.5	83.7	-128.7

^a The energy of formation was computed at the RHF/PM3 level and the dihedral angle values were calculated at the RHF/PM3/3–21G* *ab initio* level.

UV–visible spectroscopy

From the three-dimensional contour plotting of the molecular orbital (Plate 2), the nature of the chromophore mainly involved in the HOMO–LUMO electronic transition on the UV–visible spectra of **1** and **2** may be predicted.

For **1** and **2**₁, the HOMO → LUMO transition does not appear as specific to a peculiar part of the molecule and induces a drastic change in the electronic distribution on the whole flavone moiety, notably on the γ -pyrone ring.

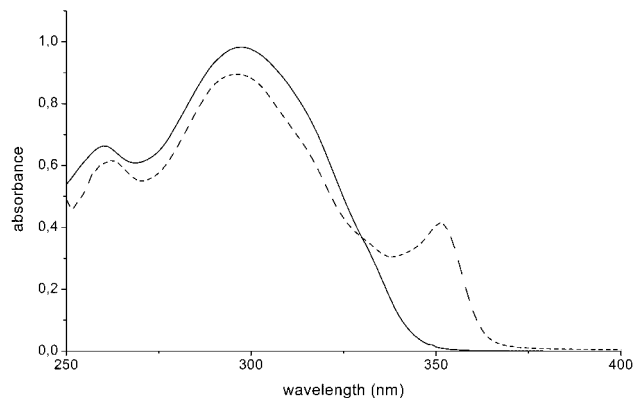


Figure 4. Electronic absorption spectra of **2** ($4 \times 10^{-5} \text{ mol l}^{-1}$) dissolved in DMSO (dashed line) and methanol (full line)

As reported previously for flavone,¹⁵ the inter-ring bond that exhibits a π antibonding character in the HOMO adopts a bonding character in the LUMO. As far as the **2**₂ conformer is concerned, the electronic density in the HOMO appears localized on the terminal D ring and the HOMO \rightarrow LUMO transition is expected to be characteristic of an intramolecular charge-transfer band from the D ring towards the entire flavonoic moiety (Plate 3). If the HOMO–LUMO energy gap is quasi-equal for **2**₁ and **2**₂, the electronic nature of the transition is largely controlled by the molecular conformation.

As in solution many conformational structures may co-exist (depending also on the solvent properties), the band arising at higher wavelengths in the UV–visible spectrum is expected to be complex. The electronic absorption spectra of **2** ($4 \times 10^{-5} \text{ mol l}^{-1}$) in methanol and in dimethyl sulphoxide (DMSO) are presented in Fig. 4. A large and strong absorption pattern centered experimentally at 297 nm appearing in both solvents surely corresponds to the HOMO–LUMO transition of π – π^* character. Nevertheless, in DMSO, an additional band at 352 nm clearly arises, indicating that solvation of the solute particularly influences the electronic spectra of this kind of flexible molecule.

Table 4. ESR hyperfine splitting constants (G) and proton assignment (number, in parentheses)

Compound	A1	A2
BHT	1.56 (2)	11.5 (3)
1	2.15 (2)	
2	2.13 (2)	

ESR spectroscopy

ESR spectroscopic experiments using the cerium(IV) oxidation system showed the ability of **1** and **2** to form a phenoxy radical. These results were compared with those for the BHT reference for which the hyperfine splitting constants are close to those found in the literature.¹⁶ The hyperfine splitting constants are given in Table 4 and the related spectra (experimental and simulated) are displayed in Fig. 5 for BHT and **2** respectively. For BHT the spectrum gives four packets of three lines due to the electron coupling with the two hydrogen atoms of the ring and that of the methyl group. For **1** and **2**, the spectra consist of three lines due to two hydrogen atoms coupled with the electron centered on the oxygen atom.

We have recently reported results related to the biological activities of **1** and **2** on the inhibition of copper ion or AAPH (2,2'-azobis-(2-amidinopropane) dihydrochloride)-induced LDL oxidation.¹⁷ In this paper, we have shown that **2** was 10 times more active than BHT whereas **1** showed the same activity as BHT. These results can be correlated with the theoretical HOMO and LUMO energies calculated and band gap energy ($E_{\text{HOMO}} - E_{\text{LUMO}}$) shown in Table 5. Effectively, we can see that the lowest band gap and the highest activity were observed with 0.9 and 1.7 eV differences, respectively, comparing BHT with **2** and **1** with **2**. The major differences in band gap energy are principally supported by the LUMO energy values, which are 1.7 and 2.7 eV higher for BHT and **1**, respectively, compared with the **2** active one. In another part the HOMO energy value is 0.5 eV lower for **2**.

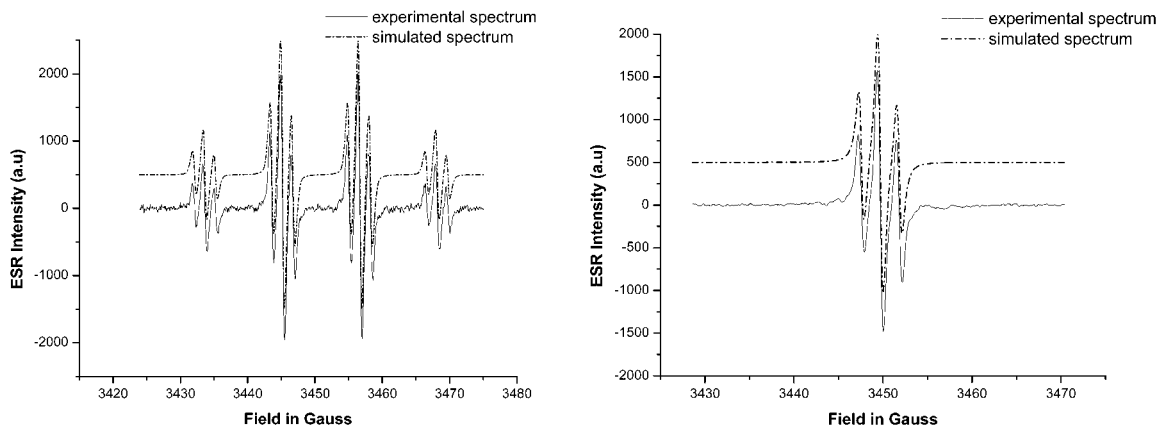


Figure 5. Experimental and simulated ESR spectra of BHT (left) and **2** (right) radical formed by oxidation with the Ce(IV) system. Experimental settings were amplitude modulation 1 G, microwave power 1 mW and receiver level gain 2×10^4

Table 5. HOMO and LUMO energy values

	E_{HOMO} (eV)	E_{LUMO} (eV)	Band gap (eV)
BHT	-8.50	0.95	-9.45
1	-8.27	1.96	-10.23
2 ₁	-9.26	-0.70	-8.57
2 ₂	-9.4	-0.73	-8.67

Previous studies with other flavonoid compounds such as quercetin and taxifolin have shown that the formation of a phenoxy radical occurs with maximum spin density (84%) localized on the oxygen when a hydrogen radical is removed. Calculation of spin densities with the **1** and unfolded **2**₁ phenoxy species revealed a distribution of spin densities on the D ring with a higher value on the oxygen (34%). In this case the SOMO (singly occupied molecular orbital) is localized at the spin density site. By contrast, for the folded **2**₂, the spin densities are also distributed on the D ring whereas the SOMO is mainly localized on the A ring on carbon 3. The SOMO energy is close to the LUMO energy, indicating the presence of a reactive site for the scavenging mechanism. We have previously shown that carbon at the 3-position is the preferential site of hydroxylation in basic aqueous solution.¹³ In order to confirm our hypothesis, we performed mass spectrometric analysis of **2** after initiation of phenoxy radical with cerium(IV) in the presence of a small amount of NaOH. We can observe mainly two peaks at m/z 583 ($M+H$)⁺ and m/z 604 ($M+Na$)⁺, which are related to the molecular ion peaks of the molecule. An additional peak at m/z 598 is also observed, which can be attributed to an oxygen addition resulting from hydroxylation of the molecule.

CONCLUSION

The modified analogues of the natural flavones **1** and **2** have been fully characterized in the solid state and in solution. The crystallographic structure of **1** displays particular hydrogen bonding networks and that of **2** presents some strong π - π interactions, allowing the stabilization of the crystal lattice. Theoretical calculations have shown that **2** can adopt a folded conformation in solution. Interestingly, **2** is 12 and three time more active than **1** and quercetin (a well-known antioxidant flavonoid), respectively, in the LDL lipid peroxidation test.¹⁷ Antioxidant activity and, in particular, inhibition of lipid peroxidation is a multi-factor event. The ability of radical formation, stabilization of the radicals, capability of metal chelation and lipophilicity remain important factors for the inhibitory activity. In this study we focused on the electronic behavior of these two compounds and the radical stabilization properties since **1** and **2** do not complex copper and their lipophilicity is of the same

order (HPLC retention times 73.31 and 79.22 min, respectively). Oxidation of **1** and **2** by cerium(IV) gives the same radical species, which are stable in the course of time. Nevertheless, the role of the D ring in the electronic behavior indicates that it seems to be responsible for the antioxidant properties. The major difference that explains this reactivity is the observed band gap energy value principally supported by the LUMO energy value. These results open the route towards the rational design of new antioxidant leads.

EXPERIMENTAL

Synthesis

TLC analyses were performed on a 3 × 10 cm plastic sheet precoated with silica gel 60F254 (Merck) with the solvent system ethyl acetate-hexane (1:4). SiO₂ (200–400 mesh) (Merck) was used for column chromatography. Melting-points were obtained on a Reichert Thermopan melting-point apparatus, equipped with a microscope and are uncorrected. Infrared spectra were obtained on a Perkin-Elmer 881 spectrometer on KBr pellets. NMR spectra were obtained at 25°C on a Bruker AC 200 spectrometer, for ¹H at 200 MHz and for ¹³C at 50 MHz. Chemical shifts are indirectly referenced to TMS via the solvent signal (chloroform-*d*₁ 7.26 and 77.0 ppm; DMSO-*d*₆ 2.50 and 39.5 ppm). *J* values are given in Hz. Mass spectra were recorded on a Finnigan MAT Vision 2000 spectrometer [for matrix-assisted laser desorption/ionization (MALDI)]. Elemental analyses were performed at CNRS Laboratories (Vernaison) and were within 0.4% of the theoretical value.

Diester 3. A 1.7 g (12.5 mmol) amount of 2-hydroxyacetophenone, 5.12 g (19 mmol) of 3,5-di-*tert*-butyl-4-hydroxybenzoyl chloride and 0.122 g of 4-dimethylaminopyridine were dissolved in 50 ml of dry pyridine and the stirred mixture was heated at 60°C for 2 h under an atmosphere of argon. The solution was cooled and 200 ml of water were added. The solid was filtered and washed with water until the pH was 7. The solid was dried and crystallized from ethanol to give 1.94 g of the diester **3** (34% yield). Elemental analysis for C₃₈H₄₈O₆, calculated C 75.97, H 8.05, O 15.98, found C 76.14, H 8.21, O 15.51%; m.p. = 227°C; infrared (ν/cm^{-1}), 3580 (ν phenolic OH), 2880 (ν C-H), 1725 (ν C=O ester), 1700 (ν C=O ketone), 1600 (ν C=C aromatic); ¹H NMR (CDCl₃), δ 1.38 [18H, s, 2 × C (CH₃)₃], 1.49 [18H, s, 2 × C (CH₃)₃], 2.59 (3H, s, COCH₃), 5.91 (1H, bs, OH), 7.25 (1H, dd, ³*J* = 8.3 Hz, ⁴*J* = 1.6 Hz, H3), 7.35 (1H, td, ³*J* = 8.3 Hz, ⁴*J* = 1.6 Hz, H5), 7.58 (1H, td, ³*J* = 8.3 Hz, ⁴*J* = 1.6 Hz, H4), 7.86 (1H, dd, ³*J* = 8.3 Hz, ⁴*J* = 1.6 Hz, H6), 8.08 (2H, s, ring B or D), 8.22 (2H, s, ring B or D); MALDI + MS, m/z 623.2 ($M+Na$), 639.2 ($M+K$).

Diarylpropane-1,3-dione 4. A 2.25 g (37.5 mmol) amount of diester **3** and 1.5 g (37.5 mmol) of sodium hydroxide (granulometry: 20–40 mesh) were dissolved in 60 ml of dry DMSO and the mixture was stirred at room temperature for 2 h. The solution was poured into 200 ml of ice-water. Acetic acid was added until the pH was 7. The solid was filtered and washed with water. The solid was dried and crystallized from ethanol to give 1.62 g of diarylpropane-1,3-dione **4** (72% yield). Elemental analyses for $C_{38}H_{48}O_6$, calculated C 75.97, H 8.05, O 15.98; found C 75.58, H 8.32, O 15.63%; m.p. = 190°C; infrared (ν/cm^{-1}), 3620 (ν phenolic OH), 2880 (ν C–H), 1740 (ν C=O ester), 1690 (ν C=O ketone), 1600 and 1560 (ν C=C aromatic); 1H NMR ($CDCl_3$), δ 1.38 [18H, s, $2 \times C(CH_3)_3$], 1.51 [18H, s, $2 \times C(CH_3)_3$], 5.82 (1H, bs, phenolic OH), 6.80 (1H, bs, ethylenic H), 6.97 (2H, m, H6 and H4), 7.48 (1H, td, $^3J = 8.4$ Hz, $^4J = 1.5$ Hz, H5), 7.76 (1H, dd, $^3J = 8.4$ Hz, $^4J = 1.5$ Hz, H3), 7.93 (2H, s, ring B or D), 8.09 (2H, s, ring B or D), 12.05 (1H, bs, phenolic OH), 14.5 (1H, bs, enolic OH); MALDI + MS, m/z 623.1 (M + Na), 639.0 (M + K).

Flavone 2. A 1 g (1.7 mmol) amount of diarylpropane-1,3-dione **4** was dissolved in 200 ml of acetic acid and 8 ml of sulfuric acid and the stirred mixture was refluxed for 1 h. The solution was cooled and 200 ml of water were added. The solid was filtered and washed with water until pH = 7. The solid was dried and crystallized from ethanol to give 0.62 g of **2** (65% yield). Elemental analyses for $C_{38}H_{46}O_5$, calculated C 78.32, H 7.96, O 13.72; found C 78.45, H 8.04, O 13.52%; m.p. = 240°C; infrared (ν/cm^{-1}), 3620 (ν phenolic OH), 2880 (ν C–H), 1740 (ν C=O ester), 1690 (ν C=O ketone), 1600 and 1560 (ν C=C aromatic); 1H NMR ($CDCl_3$), δ 1.40 [18H, s, $2 \times C \times (CH_3)_3$], 1.49 [18H, s, $2 \times C(CH_3)_3$], 5.81 (1H, bs, OH), 6.85 (1H, s, H3), 7.43 (1H, td, $^3J = 7.5$ Hz, $^4J = 1.2$ Hz, H6), 7.61 (1H, dd, $^3J = 8.8$ Hz, $^4J = 1.2$ Hz, H8), 7.71 (1H, td, $^3J = 7.7$ Hz, $^4J = 1.2$ Hz, H7), 7.91 (2H, s, ring B), 8.08 (2H, s, ring D) 8.26 (1H, dd, $^3J = 8.0$ Hz, $^4J = 1.6$ Hz, H5); ^{13}C NMR ($CDCl_3$), δ 30.2 [C (CH_3)₃], 31.4 [C (CH_3)₃], 34.4 [C (CH_3)₃], 35.8 [C (CH_3)₃], 107.5 (C3), 118.2 (C8), 121.1 (C1''), 124.0 (C4a), 124.5 (C2'), 125.2 (C5), 125.7 (C6), 128.0 (C2''), 128.4 (C1'), 133.6 (C7), 136.2 (C3''), 144.2 (C3'), 151.7 (C4'), 156.3 (C8a), 158.7 (C4''), 164.1 (C2), 168.6 (Cc), 178.6 (C4); MALDI + MS, m/z 583.4 (M + H), 605.3 (M + Na).

Flavone 1. A 1.0 g (1.7 mmol) amount of **2** and 1.0 g (25 mmol) of sodium hydroxide were dissolved in 40 ml of dry DMSO and the stirred mixture was heated at 60°C for 2 h under an atmosphere of argon. The solution was cooled and 200 ml of water were added. The solid was filtered and washed with water until the pH was 7. The solid was dried and crystallized from ethanol to give 0.32 g of **1** (53% yield). Elemental analyses for $C_{23}H_{26}O_3$, calculated C 78.83, H 7.48, O 13.69, found

C 78.48, H 7.43, O 13.81%; m.p. = 240°C; infrared (ν/cm^{-1}), 3450 (ν phenolic OH), 2980 (ν C–H), 1620 (ν C=O ketone), 1590 and 1570 (ν C=C aromatic); 1H NMR ($CDCl_3$), δ 1.55 [18H, s, $2 \times C(CH_3)_3$], 5.70 (1H, bs, OH), 6.80 (1H, s, H3), 7.45 (1H, td, $^3J = 7.5$ Hz, $^4J = 1.2$ Hz, H6), 7.61 (1H, dd, $^3J = 8.8$ Hz, $^4J = 1.2$ Hz, H8), 7.73 (1H, td, $^3J = 7.7$ Hz, $^4J = 1.2$ Hz, H7), 7.80 (2H, s, ring B), 8.26 (1H, dd, $^3J = 8.0$ Hz, $^4J = 1.6$ Hz, H5); ^{13}C NMR ($CDCl_3$), δ 30.2 [C (CH_3)₃], 34.6 [C (CH_3)₃], 106.2 (C3), 118.1 (C8), 122.8 (C1'), 123.7 (C4a), 124.0 (C2'), 125.1 (C5), 125.7 (C6), 133.5 (C7), 136.7 (C3'), 156.3 (C8a), 157.3 (C4'), 164.8 (C2), 178.6 (C4); MALDI + MS, m/z 351.3 (M + H), 373.3 (M + Na), 389.3 (M + K).

NMR NOE measurements

1H NMR spectra of **1** and **2**, dissolved in DMSO- d_6 solution (2.5 mg ml $^{-1}$), were recorded on a Bruker AC 200 spectrometer equipped with an Aspect 3000 computer operating in the Fourier transform mode with quadrature detection at 200 MHz using tetramethylsilane (TMS) as the internal reference. One-dimensional NOE values were obtained in the difference mode by subtracting two types of spectra, one in which the desired signal was saturated at low power for 30 s and the other in which the off irradiation was out of the spectrum. The steady state was obtained with two dummy scans. Homonuclear Overhauser effect experiments on **1** and **2** gave the following results: irradiation of the hydrogen H3 at 6.80 ppm (**1**) or 6.85 ppm (**2**) produced NOEs of 32% and 27%, respectively, of aromatic hydrogens of the B ring and irradiation of the aromatic hydrogens H2' and H6' at 7.80 ppm (**1**) and 7.91 ppm (**2**) induced NOEs of 37% and 34%, respectively, of the hydrogen H3. Most commonly, intense NOEs correspond to short distances (1.8–2.7 Å).

ESR spectroscopy

ESR spectroscopy was performed on a Bruker ELEXYS 580^E spectrometer operating at 9.7 GHz and 100 kHz frequency modulation. Amplitude modulation and microwave power were set at 0.8 G and 1 mW, respectively. Radical generation was carried out by using the cerium(IV) oxidant procedure.¹⁸ Spectrum simulation was performed with Bruker Simfonia software.

X-ray diffraction

X-ray diffraction measurements were performed on a Bruker AXS three-circle diffractometer equipped with a charge-coupled device (CCD) two-dimensional detector (λ Mo $K\alpha = 0.71069$ Å, graphite monochromator,

T = 294 K). An empirical absorption correction was applied by using the SADABS program. Structure solution was achieved by the direct method (SHELXS-86) and refinement by using the full-matrix least-squares techniques (SHELXTL program). All hydrogen atoms were found on a Fourier difference map and their positions refined, their thermal parameter being fixed at 1.2, the value of the equivalent thermal parameter of the atom to which they are bound. The experimental parameters for **1** and **2** are summarized in Table 1.

Mass spectrometry

MALDI mass spectra were measured on a Finnigan MAT (Bremen) Vision 2000 instrument. The matrix used was dihydroxybenzoic acid–water.

Computational method

All calculations were performed on an NT workstation (PIII 650 MHz processor) using the Spartan Pro V 1.0.2 software package. A conformational analysis was initially investigated for both molecules **1** and **2** using the Monte Carlo method implemented in Spartan. Subsequently, the energies and structures of the more stable conformers were minimized using the MMF94 force field and fully optimized at the *ab initio* level RHF/3–21G*.

The electronic absorption spectra were calculated at the optimized geometry with the configuration interaction (CI) ZINDO/S method that is well parameterized to reproduce UV–visible spectroscopic transitions. The CI calculations were performed by taking into account the 13 highest occupied molecular orbitals (HOMOs) and the 13 lowest unoccupied molecular orbitals (LUMOs).

Electronic absorption spectroscopy

The UV–visible absorption spectra of **1** and **2** dissolved in DMSO were recorded on a Varian Cary 1 double-beam spectrophotometer in the 200–500 nm range with 2 nm spectral resolution.

REFERENCES

1. Rump AF, Schussler M, Acar D, Cordes A, Ratke R, Theisohn M, Rosen R, Klaus W, Fricke U. *Gen. Pharmacol.* 1995; **26**: 603–611.
2. Tzeng SH, Ko FN, Teng CM. *Thromb. Res.* 1991; **64**: 91–100.
3. Ferrandiz M, Alcaraz MJ. *Agents Actions* 1991; **32**: 283–288.
4. Middleton E Jr, Kandaswami C. *Biochem. Pharmacol.* 1992; **43**: 1167–1179.
5. Terao J, Piskula M, Yao Q. *Arch. Biochem. Biophys.* 1994; **308**: 278–284.
6. Laughton MJ, Evans PJ, Moroney MA, Houlst JRC, Halliwell B. *Biochem. Pharmacol.* 1991; **42**: 1673–1681.
7. Siess MH, Leclerc J, Canivenc-Lavier MC, Rat P, Suschetet M. *Toxicol. Appl. Pharmacol.* 1995; **130**: 73–78.
8. Cotellet N, Bernier JL, Catteau JP, Pommery J, Wallet JC, Gaydou EM. *Free Rad. Biol. Med.* 1996; **20**: 35–43.
9. Cushman M, Nagarathnam D, Burg DL, Geahlen RL. *J. Med. Chem.* 1991; **34**: 798–806.
10. Nagao M, Morita N, Yahagi T, Shimizu M, Kuroyanagi M, Fukuoka M, Yoshihira K, Natori S, Fujino T, Sugimura T. *Environ. Mutagen.* 1981; **3**: 401–419.
11. Elliger GA, Henika PR, MacGregor JT. *Mutat. Res.* 1984; **135**: 77–86.
12. Lebeau J, Nevière R, Cotellet N. *Bioorg. Med. Chem. Lett.* 2001; **11**: 23–27.
13. Cotellet N, Bernier JL, Catteau JP, Gaydou E, Wallet JC. *Free Rad. Biol. Med.* 1992; **13**: 211–219.
14. Rice-Evans CA, Packer L. *Flavonoids in Health and Disease*. Marcel Dekker: New York, 1998; 221.
15. Vrielynck L, Cornard JP, Merlin JC, Bopp P. *J. Mol. Struct.* 1993; **297**: 227–234.
16. Pedersen JA. *Handbook of EPR Spectra from Quinones and Quinols*. CRC Press: Boca Raton, FL, 1985.
17. Lebeau J, Furman C, Bernier JL, Duriez P, Teissier E, Cotellet N. *Free Rad. Biol. Med.* 2000; **29**(9): 900–912.
18. Dixon WT, Foster WEJ, Murphy D. *J. Chem. Soc., Perkin Trans. 2* 1973; 2124–2127.